# Unidirectional surface plasmon-polariton excitation by a compact slot partially filled with dielectric

**Dongdong Li,[1] Dao Hua Zhang,[1,*] Changchun Yan,[2] Tao Li,[3] Yueke Wang,[1] Zhengji Xu,[1] Jun Wang,[1] and Fei Qin[1]**

[1]*School of Electrical and Electronic Engineering, Nanyang Technological University, 639798 Singapore*
[2]*School of Physics and Electronic Engineering, Xuzhou Normal University, 221116 China*
[3]*College of Engineering and Applied Sciences, Nanjing University, 210093 China*
[*]*edhzhang@ntu.edu.sg*

**Abstract:** We propose a new scheme on unidirectional surface plasmon-polariton (SPP) excitation with the following advantages: ultracompact size, working at arbitrary incidence angle and over a wide spectrum. The proposed structure utilizes a partially filled metallic slot with dielectric to realize unidirectional SPP excitation via direct field manipulation. We theoretically and numerically show that unidirectional SPP excitation with a ratio of 93% can be achieved by a structure with a 50 nm slot. The proposed structure keeps its functional capability over incident angles from −80° to 80°, and has a broadband working spectrum of more than 70 nm.



**OCIS codes:** (240.0240) Optics at surfaces; (240.6680) Surface plasmons.

## References and links

1. W. L. Barnes, A. Dereux, and T. W. Ebbesen, "Surface plasmon subwavelength optics," Nature **424**(6950), 824–830 (2003).
2. S. A. Maier, *Plasmonics: Fundamentals and applications* (Springer, 2007), Chap. 2.
3. S. A. Maier, P. G. Kik, H. A. Atwater, S. Meltzer, E. Harel, B. E. Koel, and A. A. G. Requicha, "Local detection of electromagnetic energy transport below the diffraction limit in metal nanoparticle Plasmon waveguides," Nat. Mater. **2**(4), 229–232 (2003).
4. C. Yan, D. H. Zhang, and D. Li, "Wedge-shaped metal-dielectric composite metamaterials for light control," Metamaterials (Amst.) **4**(4), 170–174 (2010).
5. B. Steinberger, A. Hohenau, H. Ditlbacher, F. R. Aussenegg, A. Leitner, and J. R. Krenn, "Dielectric stripes on gold as surface plasmon waveguides: Bends and directional couplers," Appl. Phys. Lett. **91**(8), 081111 (2007).
6. J. S. Q. Liu, R. A. Pala, F. Afshinmanesh, W. Cai, and M. L. Brongersma, "A submicron plasmonic dichroic splitter," Nat Commun **2**, 525 (2011).
7. C. Yan, D. H. Zhang, Y. Zhang, D. Li, and M. A. Fiddy, "Metal-dielectric composites for beam splitting and far-field deep sub-wavelength resolution for visible wavelengths," Opt. Express **18**(14), 14794–14801 (2010).
8. B. Wang, L. Aigouy, E. Bourhis, J. Gierak, J. P. Hugonin, and P. Lalanne, "Efficient generation of surface plasmon by single-nanoslit illumination under highly oblique incidence," Appl. Phys. Lett. **94**(1), 011114 (2009).
9. Y. Wang, L. Wang, J. Liu, X. Zhai, L. Wang, D. Xiang, Q. Wan, and B. Meng, "Plasmonic surface-wave bidirectional splitter in different angles of incident light," Opt. Commun. **283**(9), 1777–1779 (2010).
10. J. Chen, Z. Li, S. Yue, and Q. Gong, "Efficient unidirectional generation of surface plasmon polaritons with asymmetric single-nanoslit," Appl. Phys. Lett. **97**(4), 041113 (2010).
11. N. Bonod, E. Popov, L. Li, and B. Chernov, "Unidirectional excitation of surface plasmons by slanted gratings," Opt. Express **15**(18), 11427–11432 (2007).
12. A. Roszkiewicz and W. Nasalski, "Unidirectional SPP excitation at asymmetrical two-layered metal gratings," J. Phys. B **43**(18), 185401 (2010).
13. A. Baron, E. Devaux, J. C. Rodier, J. P. Hugonin, E. Rousseau, C. Genet, T. W. Ebbesen, and P. Lalanne, "Compact antenna for efficient and unidirectional launching and decoupling of surface plasmons," Nano Lett. **11**(10), 4207–4212 (2011).
14. F. López-Tejeira, S. G. Rodrigo, L. Martín-Moreno, F. J. García-Vidal, E. Devaux, T. W. Ebbesen, J. R. Krenn, I. P. Radko, S. I. Bozhevolnyi, M. U. González, J. C. Weeber, and A. Dereux, "Efficient unidirectional nanoslit couplers for surface plasmons," Nat. Phys. **3**(5), 324–328 (2007).
15. T. Xu, Y. Zhao, D. Gan, C. Wang, C. Du, and X. Luo, "Directional excitation of surface plasmons with subwavelength slits," Appl. Phys. Lett. **92**(10), 101501 (2008).

#180265 - $15.00 USD Received 21 Nov 2012; revised 15 Feb 2013; accepted 17 Feb 2013; published 4 Mar 2013

16. Y. Wang, L. Wang, J. Liu, X. Zhai, L. Wang, D. Xiang, Q. Wan, and B. Meng, "Plasmonic surface-wave bidirectional splitter in different angles of incident light," Opt. Commun. **283**(9), 1777–1779 (2010).
17. L. Wang, T. Li, L. Li, W. Xia, X. G. Xu, and S. N. Zhu, "Electrically generated unidirectional surface plasmon source," Opt. Express **20**(8), 8710–8717 (2012).
18. A. Baron, E. Devaux, J. C. Rodier, J. P. Hugonin, E. Rousseau, C. Genet, T. W. Ebbesen, and P. Lalanne, "Compact antenna for efficient and unidirectional launching and decoupling of surface plasmons," Nano Lett. **11**(10), 4207–4212 (2011).
19. M. He, J. Liu, K. Wang, X. Wang, and Z. Gong, "Efficient directional excitation of surface plasmon polaritons by partial dielectric filling slit structure," Opt. Commun. **285**(21-22), 4588–4592 (2012).
20. S. B. Raghunathan, C. H. Gan, T. van Dijk, B. Ea Kim, H. F. Schouten, W. Ubachs, P. Lalanne, and T. D. Visser, "Plasmon switching: Observation of dynamic surface plasmon steering by selective mode excitation in a sub-wavelength slit," Opt. Express **20**(14), 15326–15335 (2012).
21. X. Li, Q. Tan, B. Bai, and G. Jin, "Tunable directional beaming assisted by asymmetrical SPP excitation in a subwavelength metallic double slit," Chin. Opt. Lett. **10**(5), 052401–052403 (2012).
22. J. Chen, Z. Li, S. Yue, and Q. Gong, "Efficient unidirectional generation of surface plasmon polaritons with asymmetric single-nanoslit," Appl. Phys. Lett. **97**(4), 041113 (2010).
23. W. L. David and W. R. Hunter, "Silver (Ag)," and "Chromium (Cr)," in *Handbook of Optical Constants of Solids,* E. D. Palik, ed. (Academic, Orlando, Fla., 1985).
24. T. Bååk, "Silicon oxynitride; a material for GRIN optics," Appl. Opt. **21**(6), 1069–1072 (1982).
25. R. A. Chipman, "Optical and physical properties of materials," in *Handbook of Optics*, M. Bass, ed. (McGraw-Hill, New York, 1995).
26. J. R. Devore, "Refractive indices of rutile and sphalerite," J. Opt. Soc. Am. **41**(6), 416–419 (1951).
27. S. Astilean, Ph. Lalanne, and M. Palamaru, "Light transmission through metallic channels much smaller than the wavelength," Opt. Commun. **175**(4-6), 265–273 (2000).
28. P. Lalanne, J. P. Hugonin, and J. C. Rodier, "Theory of surface plasmon generation at nanoslit apertures," Phys. Rev. Lett. **95**(26), 263902 (2005).
29. R. F. Oulton, V. J. Sorger, D. A. Genov, D. F. P. Pile, and X. Zhang, "A hybrid plasmonic waveguide for subwavelength confinement and long-range propagation," Nat. Photonics **2**(8), 496–500 (2008).
30. M. W. Maqsood, R. Mehfuz, and K. J. Chau, "High-throughput diffraction-assisted surface-plasmon-polariton coupling by a super-wavelength slit," Opt. Express **18**(21), 21669–21677 (2010).
31. I. Avrutsky, R. Soref, and W. Buchwald, "Sub-wavelength plasmonic modes in a conductor-gap-dielectric system with a nanoscale gap," Opt. Express **18**(1), 348–363 (2010).
32. Q. Xu, V. R. Almeida, R. R. Panepucci, and M. Lipson, "Experimental demonstration of guiding and confining light in nanometer-size low-refractive-index material," Opt. Lett. **29**(14), 1626–1628 (2004).
33. K. Y. Kim, *Plasmonics - Principles and Applications* (InTech Rjieka Croatia 2012), Chap. 6.

## 1. Introduction

Surface plasmon-polariton (SPP) have received much attention for their ability to confine electromagnetic energy below the diffraction limit [1,2]. The ultimate confinement ability of SPPs makes it possible to bridge the gap between nanoelectronic and microphotonic devices for integrated hybrid chips. Over the past decades, tremendous progress has been made in developing functional SPP components. Many plasmonic devices such as waveguide [3,4], couplers [5] and splitters [6,7] have been proposed.

As one of the key components in photonic circuits, SPP generator plays a very important role. To explore the full potential of SPP, it is necessary to control both its propagation direction and strength, and efficient unidirectional SPP source is a common requirement for plasmonic integrations. A simple way to realize unidirectional SPP excitation is applying an oblique incidence [8,9]. However, in many cases, oblique incidence may not be an option due to complexity of the optical system. Unidirectional SPP excitation can be achieved under normal incidence by breaking the symmetry of a single slit or grating [10–14]. Structures consist of two parallel slits filled with different dielectrics have also shown capable of unidirectional SPPs excitation [15,16]. A variety of other schemes have been proposed for unidirectional lunching of SPPs [17–21]. These previous works greatly accelerated the development of functional SPP devices. However, as many of these devices rely on the interference of two different SPP sources generated by additional periodical structures or cavities, their dimensions are too large compared with their electronic counterparts. So far, the most compact scheme for unidirectional SPP excitation is the asymmetric single nanoslit with a lateral dimension of 370 nm [22]. In addition, as most of devices on unidirectional SPP excitation take the incident angle as the input parameter, their performance will be affected by the incident angle. In real applications, the incident angle may not always be fixed in the

#180265 - $15.00 USD Received 21 Nov 2012; revised 15 Feb 2013; accepted 17 Feb 2013; published 4 Mar 2013

normal direction. Thus, a good unidirectional SPP generator should also avoid the dependence on the incident angle.

To address these issues, we propose a new scheme to achieve efficient unidirectional SPP excitation. The proposed scheme has an extremely small size (about 50 nm of its lateral size), works over a broad spectrum and at nearly arbitrary incidence angle.

## 2. Structure and working principle

The schematic of proposed structure with labeled dimensions and materials is shown in Fig. 1(a). It consists of a silver (Ag) slab covered by a chromium (Cr) mask on which a partially filled slot is opened. The substrate and the ambient environment are modeled as the high-index dielectric and air, respectively. The structure can be divided into two functional blocks, as shown in Fig. 1(b). The first block resembles a partially filled metal-insulator-metal MIM slot structure which is primarily used to control the SPPs propagation direction. It manipulates the field distribution inside the low-index (air) and high-index (dielectric) regions, so that more energy is confined in the air region. The second block is a thin silver layer located beneath the slot waveguide and it controls the strength of the excited SPPs at the air/Ag and dielectric/Ag interfaces. By carefully selecting the wavelength, the SPPs excited at the dielectric/Ag interface can be much stronger than that excited at the air/Ag interface. When the two functional blocks are combined together, the energy confined inside the air region can be effectively coupled with the SPPs excited at the dielectric/Ag interface. Due to the asymmetric arrangement of the air region and dielectric region, the SPPs excited at the dielectric/Ag interface almost only contain wave vectors pointing to the positive *x*-axis direction.

The idea is schematically illustrated in Fig. 1(b). When a plane wave is illuminated on the slot, the incident wave is scattered by the slot and generates high spatial frequency components with $k_{x\_incident} >> k_0$, where $k_{x\_incident}$ and $k_0$ are the transverse wave vector of the scattered wave and the free space wave vector, respectively. Due to the high refractive index contrast ratio between the air and high-index dielectric, the scattered waves are mainly confined in the air region and they contain transverse wave components pointing to both positive *x*-axis and negative *x*-axis directions. Since the high-index region is located on the right hand side of the air region, for the scattered waves confined in the air region, only these waves with the transverse wave vector pointing to positive *x*-axis can reach the dielectric/Ag interface. If these wave components can provide sufficient transverse wave vectors to excite SPPs at the dielectric/Ag interface, the exited SPPs will have a propagation direction along the positive *x*-axis. Next, when the SPPs excited the dielectric/Ag interface are coupled with the plasmon modes excited at the output surface, they also propagate along the positive *x*-axis direction. As the scheme only relies on the geometric manipulation of the field distribution to excite SPPs in the desired direction, it can be scaled down to an extremely small size and works with arbitrary incidence angle.

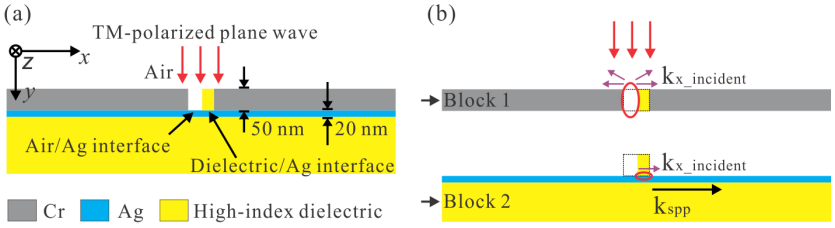


Fig. 1. Structure (a) and working principle (b) of the proposed scheme for unidirectional lunching of SPPs.

## 3. Simulation and discussion

The structure in Fig. 1(a) is numerically investigated by the Radio Frequency (RF) module of COMSOL Multiphysics 3.5a in frequency domain. The simulation domain has a dimension of

#180265 - $15.00 USD Received 21 Nov 2012; revised 15 Feb 2013; accepted 17 Feb 2013; published 4 Mar 2013

5000 nm × 5000 nm with perfectly matched layers (PMLs) as the boundaries to reduce the backscattered waves. To ensure the accuracy of the calculations, the maximum mash size for the regions around the slot and for the remaining regions are 0.2 nm and 1 nm, respectively. The permittivities of Ag and Cr are extracted from experimental data [23], while the permittivity of the high-index dielectric is assumed to be 4 over the spectrum of interest. In optical range, such high-index dielectric permittivity can be realized by a variety of materials such as Silicon nitride ($Si_3N_4$), Zinc oxide (ZnO) and Titanium dioxide ($TiO_2$). At 515 nm, the permittivities of the above mentioned materials are 4.123 [24], 4.16 [25] and 7.2 [26], respectively. The simulated structure has a slot width of 50 nm, and the slot is half-filled with the high-index dielectric inclusion (the filling ratio of the high-index dielectric is 50%). Figures 2(a) and 2(b) illustrate unidirectional SPP excitations when a 515 nm transverse magnetic (TM) polarized plane wave with H||*z*-axis is normally illuminated on the slot. The total energy density (named as the time averaged power flow S in COMSOL, where S is the Poynting vector which can be calculated by S = 1/2*Re(E × H*)) is used to qualify the energy distribution inside the slot. From the simulations, it can be seen that most of the electromagnetic energy is confined at the substrate/silver interface located on the right-hand side of the slot, which is a clear indication of unidirectional SPP excitation.

Next, we theoretically show that the SPPs propagation direction can be controlled by manipulating the field distribution inside the slot. Introduction of a high-index dielectric in a MIM slot will modify the local field distribution inside the slot from two aspects. Firstly, it breaks the symmetric power distribution inside the slot, resulting in more energy confinement in the air region. As shown in the inset of Fig. 2(a) and the dashed blue line in Fig. 2(c), before the incident light excites SPPs at the dielectric/Ag interface, more energy is confined in the air region. For a MIM slot without dielectric inclusion, the electric field polarized perpendicular to the air/Cr interface is restricted around the interfaces due to the high dielectric discontinuity between air and Cr. When the two interfaces of the Cr slot are brought closer together, the plasmonic waves around the two interfaces interact and the energy is almost completely confined inside the air slot [27–30]. When a high-index dielectric is added, it introduces another high dielectric discontinuity at the dielectric/air interface, which breaks the symmetrical energy distribution. Due to the continuity of the electric displacement vector at the interface, the normal component of the electric field in the air region is increased by a factor of $\varepsilon_d$, where $\varepsilon_d$ is the permittivity of the dielectric inclusion [31]. Our simulations also reveal that the higher is the contrast ratio between the air and high-index dielectric, the more is the energy confined inside air region. Similar results have been found for dielectric slot-waveguide made of high-index-contrast materials [32]. Since more energy is confined in the air region which is located on the left side of the dielectric/Ag interface, when the energy is coupled with SPPs excited at dielectric/Ag interface, the excited surface waves will have wave vector components pointing to the positive *x*-axis. In this way, we can control the propagation direction of the excited SPPs.

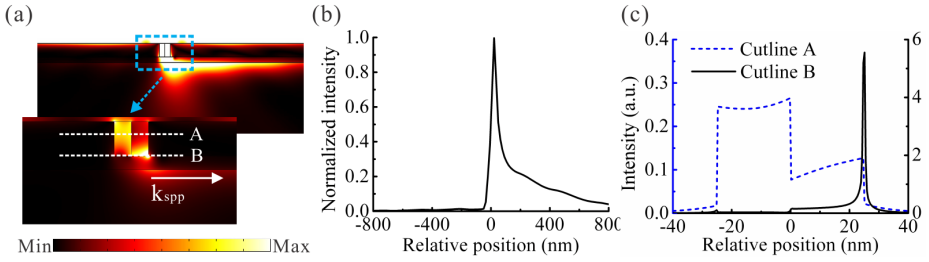


Fig. 2. Demonstration of unidirectional SPP excitation at $\lambda$ = 515 nm. The permittivties of Ag and Cr are −9.3 + 0.8i and −12.2 + 24i, respectively. (a) Energy distribution of the structure when a TM-polarized plane wave normally illuminates at the slot. Inset of the figure illustrates the energy distribution inside the slot with better contrast. (b) Normalized energy distribution at the output surface. (c) Energy distributions inside the partially filled slot. Cutline A and Cutline B are located at the plane 30 nm and 1 nm from the bottom of the slot, respectively.

#180265 - $15.00 USD Received 21 Nov 2012; revised 15 Feb 2013; accepted 17 Feb 2013; published 4 Mar 2013

Secondly, the introduction of the dielectric in a MIM slot will also affect the strength of the excited SPPs at the air/Ag and dielectric/Ag interfaces. Due to the fact that the light line is located on the left side of the SPP dispersion curve, previous research were mainly focused on SPP excitation by propagating waves with a special wave vector compensation configuration (such as prism coupling). Here we assume that the incidence itself already contains high transverse wave vector components (e.g. $k_{x\_incident} >> k_0$). By making use of the high transverse wave vector components, we show that the strength of SPPs excited at both dielectric/Ag and Air/Ag interfaces can be engineered by tuning the wavelength. To demonstrate the idea, we first study the dispersion relations of SPPs propagating at metal-dielectric interface [2]:

$$k_{spp} = k_0 \sqrt{\frac{\varepsilon_{metal}\varepsilon_{dielectric}}{\varepsilon_{dielectric} + \varepsilon_{metal}}}. \quad (1)$$

Figure 3 shows the dispersion relations of the SPPs propagating at the air/Ag and dielectric/Ag interfaces. It can be seen that, over a broad spectrum (above 380 nm), the wave vector $k_{spp\_dielectric}$ required to excite SPPs at the dielectric/Ag interface is always higher than the wave vector $k_{spp\_air}$ required to excite SPPs at the air/Ag interface. When the incidence with high wave vector components is used to excite SPPs at both interfaces, the SPPs excited at dielectric/Ag interface is much stronger than that excited at air/Ag interface due to the smaller wave vector mismatch. At peak 2 ($\lambda$ = 350 nm), however, $k_{spp\_dielectric}$ becomes smaller than $k_{spp\_air}$. In this case, the SPPs excited at air/Ag interface will be much stronger than that excited at dielectric/Ag interface. These results indicate that such a structure can selectively excite SPPs either dominated by the dielectric/Ag interface or the air/Ag interface by tuning the incident wavelength, provided that the incidence contains sufficient high wave vector components. For the proposed structure, due to the small size of the partially filled slot, the high wave vector components can be simply generated by the scattered electromagnetic waves at the partially filled slot in block 1. To quantitatively estimate the phase mismatches between the scattered light and both SPPs, we estimated the dominant transverse wave vector components of the scattered light. The spectrum of the dominant wave vector components of $k_{x\_incident}$ is plotted in Fig. 3(a). From the spectrum, it can be seen that the scattered light indeed contain high transverse wave vector components that larger than both $k_{spp\_dielectric}$ and $k_{spp\_air}$. For $\lambda$>380 nm, the wave vector mismatch between $k_{x\_incident}$ and $k_{spp\_dielectric}$ is smaller than that between $k_{x\_incident}$ and $k_{spp\_air}$. Thus the strength of the SPPs excited at the dielectric/Ag interface can be much stronger than that excited at the air/Ag interface.

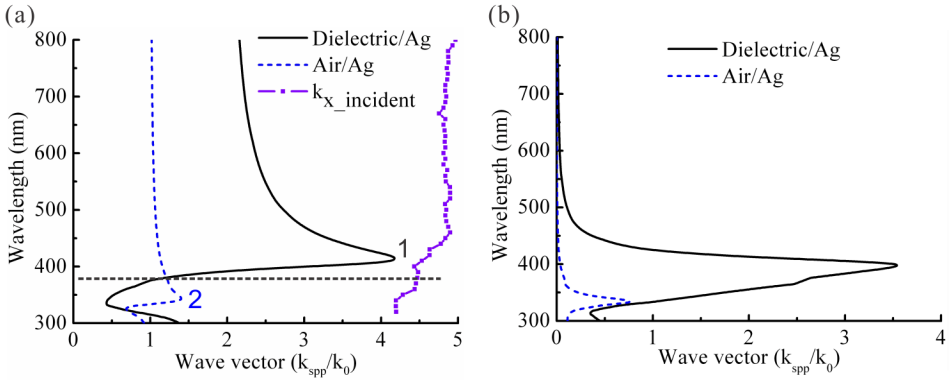


Fig. 3. Dispersion relation of SPPs at the interfaces of air/Ag (blue dashed curve) and dielectric/Ag (black solid curve), as well as the spectrum of the dominant transverse wave vector components of the scattered light (violet scatter plot). The permittivities of Ag and Cr are extracted from reference [23]. The horizontal axis and the vertical axis correspond to the real part (a) and imaginary part (b) of the wave vector and wavelength, respectively. Peaks 1 and 2 are centered at 410 nm and 350 nm, respectively.

#180265 - $15.00 USD Received 21 Nov 2012; revised 15 Feb 2013; accepted 17 Feb 2013; published 4 Mar 2013

In the previous paragraph, for simplicity, we only considered the SPPs on single dielectric/Ag or dielectric/Ag interfaces. For the proposed structure, due to the finite thickness of the Ag layer, the SPPs excited at the two interfaces of the Ag layer couple with each other and give rise to coupled plasmon modes. The SPPs considered are the SPP modes supported by the insulator-metal-insulator (IMI) structures [33]. The SPP dispersion relation of such IMI structures can be evaluated by the following equation [2]

$$e^{-2k_1 a} = \frac{k_1/\varepsilon_1 + k_2/\varepsilon_2}{k_1/\varepsilon_1 - k_2/\varepsilon_2} \cdot \frac{k_1/\varepsilon_1 + k_3/\varepsilon_3}{k_1/\varepsilon_1 - k_3/\varepsilon_3}. \quad (2)$$

where $a$ is the thickness of the metal layer, $k_1$ and $\varepsilon_1$ are the wave vector and permittivity of the metal layer, $k_2$ and $\varepsilon_2$, $k_3$ and $\varepsilon_3$ are the wave vectors and permittivities of the two insulator layers, respectively. The dispersion curves of the dielectric/Ag/dielectric and air/Ag/dielectric layers are plotted in Fig. 4. From the figure, it can be seen that the dispersion relation of the dielectric/Ag/dielectric layers splits into even and odd modes. For $\lambda$>360 nm, the dispersion curve of the dielectric/Ag/dielectric layers is at the right hand side of that of the air/Ag/dielectric layers. Due to the smaller momentum mismatch, the dominant transverse wave vector components of the scattered light will couple with the even or odd SPP modes of the dielectric/Ag/dielectric layers. In this spectrum range, the strength of the SPPs excited at the dielectric/Ag/dielectric layers can be much stronger than that excited at the air/Ag/dielectric layers. It is also found that the even mode of the dielectric/Ag/dielectric layers intersects with the dominant transverse wave vectors of the scattered light at 400 nm (intersect 1) and 510 nm (intersect 3), respectively. At these two intersecting points, the dominant incident wave vectors are perfectly matched with that required to excite the SPPs at the dielectric/Ag/dielectric layers, and thus high efficient excitation of SPPs can be achieved. While for $\lambda\approx$340 nm, the momentum mismatch between the incident wave vectors and that required to excite SPPs at the air/Ag/dielectric layers become smaller. Thus high efficient excitation of SPPs at the air/Ag/dielectric layers should be achieved around 340 nm.

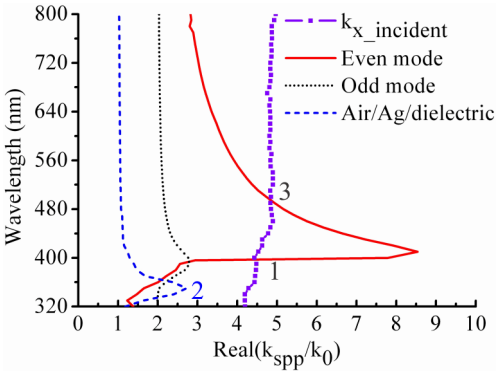


Fig. 4. Dispersion relation of SPPs at the air/Ag/dielectric layers (blue dashed curve), the dielectric/Ag/dielectric layers (even mode: red solid curve, odd mode: black dotted curve), and the spectrum of the dominant transverse wave vector components of the scattered light (violet scatter plot).

To verify the above analysis, we numerically evaluated the intensity of the electromagnetic field confined at the dielectric/Ag and air/Ag interfaces. In our simulations, the intensity is obtained by integrating the total energy confined at the dielectric/Ag and air/Ag interfaces as illustrated in Fig. 1(a). Figure 5 shows the intensities of the electromagnetic field confined at the dielectric/Ag and air/Ag interfaces with respect to the incident wavelengths ranging from 320 nm to 800 nm. At the air/Ag interface, the maximum intensity is achieved around $\lambda$ = 350 nm (peak 2), which is in good agreement with the theoretical value based on dispersion relation shown in Fig. 4. At the dielectric/Ag interface,

#180265 - $15.00 USD Received 21 Nov 2012; revised 15 Feb 2013; accepted 17 Feb 2013; published 4 Mar 2013

two peaks centered at 400 nm and 515 nm are observed. From the dispersion curves, they correspond to the two intersecting points 1 and 3 in Fig. 4, respectively.

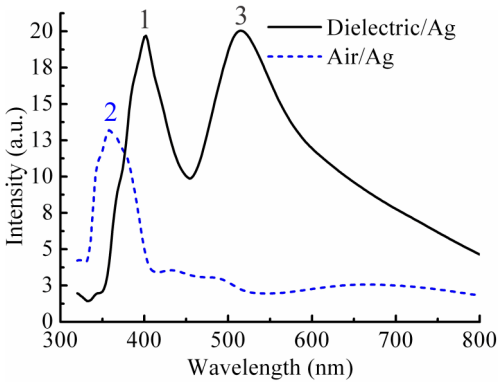


Fig. 5. Intensity of the electromagnetic field confined at the dielectric/Ag and air/Ag interfaces. Peak 1, 2 and 3 are centered at 400 nm, 350 nm and 515 nm, respectively.

Based on the above analysis, it is clear that the proposed structure is capable of unidirectional excitation of SPPs by manipulating the field distributions in the slot. In order to achieve long distance propagation, the imaginary part of the wave vector should be small. For the two SPP intensity peaks obtained at the dielectric/Ag interface, the peak at 400 nm, originated from the intrinsic SPP mode, has the imaginary part of the wave vector much larger than the peak at 515 nm (Fig. 3(b)). Therefore, the incidence at around 515 nm should have a much longer propagation distance.

To qualitatively evaluate the energy propagated in unidirectional, we evaluated the ratio $\eta = I_R/(I_R + I_L)$, where $I_R$ and $I_L$ are the intensity of the propagated SPPs at the output surface, located 500 nm and −500 nm from the center of the slot, respectively. For a 50 nm wide slot half-filled with the high-index dielectric, it is found that the ratio $\eta$ is as high as 93% for the incident wavelength of 515 nm, and an average of about 90% over a spectra ranging from 460 nm to 530 nm, as shown in Fig. 6(a). These results undoubtedly indicated that most of the transmitted energy propagate in the positive $x$-axis direction only. The broad working spectrum of the structure can be understood by the dispersion relation analysis. Since the degree of the SPPs excited at the dielectric/Ag/ dielectric layers will always be stronger than that at the air/Ag/dielectric layers for incident wave with $\lambda$>360 nm, it is not surprising that high performance unidirectional SPP excitation can be achieved over a wide spectrum. In addition, we also estimated the total efficiency of the unidirectional excitation of the SPPs, which is defined as the ratio of the energy guided through the positive $x$-axis direction over the total input energy at the slot. For a 50 nm wide slot half-filled with the high-index dielectric, the total efficiency is about 23% for the incidence of 515 nm.

To know the effect of incident angle on the unidirectional propagation, we estimated the ratio $\eta$ for the incident angles from −80° to 80° and no significant change is found in the incident range. In the numerical simulations, the 50 nm wide slot is half-filled with high-index dielectric. The incidence wavelength is fixed at 515 nm. As it can be seen from Fig. 6(b), the ratio $\eta$ only change slightly when the incident angle is varied. This is because the wave vectors used to control the direction of SPP propagation is generated by the asymmetric field distribution in the slot, and it is almost independent of the incident angle.

#180265 - $15.00 USD Received 21 Nov 2012; revised 15 Feb 2013; accepted 17 Feb 2013; published 4 Mar 2013

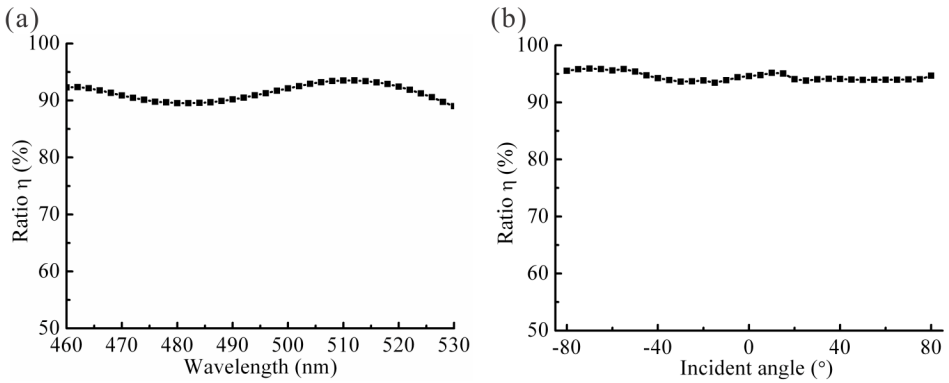


Fig. 6. Unidirectional SPPs excitation capability (measured in term of the ratio η) of the structure (a) at different wavelength. (b) at different incidence angle. The incidence wavelength is fixed at 515 nm.

Such a unidirectional SPP generator could be realized with the assistance of current nanofabrication systems such as electron beam lithography (EBL) and focused ion beam (FIB). The possible main fabrication processes are schematically illustrated in Fig. 7. These include deposition of Ag film on $Si_3N_4$ substrate, fabrication of a 50 nm wide $Si_3N_4$ layer through pattern transfer by EBL, deposition and planarization of the Cr mask layer and partial removal of $Si_3N_4$ by FIB milling.

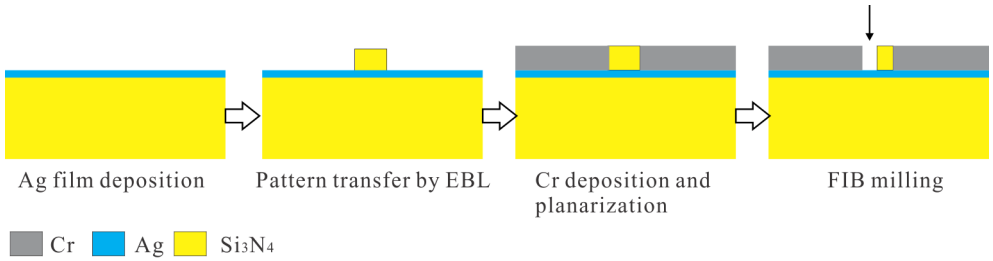


Fig. 7. Main fabrication processes of the unidirectional SPP generator.

## 3. Conclusion

In summary, we proposed a new scheme for unidirectional excitation of SPPs. The proposed structure is ultracompact and can realize unidirectional excitation in a broad incident spectrum, and is insensitive to the incidence angle. Such a scheme could help in achieving larger scale integration of all-optical devices, and has potential applications in optical communication, sensing and imaging.

## Acknowledgment

This project is supported by National Research Foundation (NRF-G-CRP 2007-01), A*Star (092154009), Singapore, AOARD, State Key Program for Basic Research of China (Nos. 2012CB921501) and National Natural Science Foundation of China (Nos. 11174136).

#180265 - $15.00 USD Received 21 Nov 2012; revised 15 Feb 2013; accepted 17 Feb 2013; published 4 Mar 2013